THE ELECTRONIC STRUCTURE OF Fe^{2+} IN REACTION CENTERS FROM *RHODOPSEUDOMONAS SPHAEROIDES*

II. Extended X-ray Fine Structure Studies

P. EISENBERGER
Bell Laboratories, Murray Hill, New Jersey 07976
M. Y. OKAMURA AND G. FEHER
University of California, San Diego, La Jolla, California 92093

ABSTRACT Extended x-ray absorption fine structure (EXAFS) studies were performed on reaction centers (RC) of the photosynthetic bacterium *Rhodopseudomonas sphaeroides* R-26. RC containing two, one, and no quinones (2Q, 1Q, 0Q) samples were studied. The average ligand distance of the first coordination shell was determined to be 2.10 ± 0.02 Å with a more distant shell at 4.14 ± 0.05 Å. The Fe^{2+} site in RC was found to have a very large structural disorder parameter, from which a spread in ligand distances per iron site of ~±0.1 Å was deduced. The most likely coordination number of the first shell is six, with a mixture of oxygens and nitrogens as ligands. The edge absorption results are consistent with the Fe^{2+} being in a distorted octahedral environment. The EXAFS spectra of the 2Q and 1Q samples with and without *o*-phenanthroline were found to be the same. This indicates that either the secondary quinone and *o*-phenanthroline do not bind to Fe^{2+} or that they replace an equivalent ligand. The 0Q sample showed a 12% decrease in the EXAFS amplitude, which was restored upon addition of *o*-phenanthroline. These results can be explained by either a loss of a ligand or a severe conformational change when the primary quinone was removed.

INTRODUCTION

The primary photochemical events in bacterial photosynthesis take place in a membrane-bound bacteriochlorophyll-protein complex called the reaction center (RC) (for a review of bacterial RC, see, for example, Feher and Okamura [1978]). Reaction centers from *Rhodopseudomonas sphaeroides* R-26 contain four bacteriochlorophylls, two bacteriopheophytins, two ubiquinones, and one Fe^{2+}. The Fe^{2+} is in a high-spin state and has not been observed to change its valence (Debrunner et al., 1975; Butler et al., 1980). It is therefore believed not to play a direct role as an electron carrier in the photosynthetic electron transfer process.

When RC are excited with light, an electron passes from a bacteriochlorophyll complex via intermediates to the primary quinone Q_1 and from there to the secondary quinone Q_2. Electron paramagnetic resonance (EPR) experiments have shown that both quinones are magnetically coupled to Fe (Wraight, 1978; Okamura et al., 1978) to form a "ferroquinone complex" (Okamura et al., 1975). These observations suggested that Fe^{2+} may be involved in the electron transfer between the quinones ("the iron wire hypothesis," Okamura et al., 1975). Preliminary evidence supporting this hypothesis came from the observation by Blankenship and Parson (1979) that the loss of Fe from RC was correlated with the loss of electron transfer from Q_1 to Q_2. Their evidence cannot be taken as conclusive, however, since the removal of iron is accompanied by dissociation of one of the protein subunits of the reaction center (Debus et al., 1981).

Very little is known about the structure of the ferroquinone complex. In the first part of this study (Butler et al., 1980), we measured the static magnetization of reaction centers with different numbers of quinones. The results were consistent with the Fe being in an octahedral environment with rhombic distortion (i.e., very low symmetry). The values of the crystalline field parameters were found to be approximately the same for reaction centers having one and two quinones. It was therefore concluded that the secondary quinone probably does not bind directly to Fe^{2+}. A similar, but less firm conclusion was reached for the primary quinone; in this case additional evidence (the similarity of the EPR spectra of $Q_1^- Fe^{2+}$ and $Q_2^- Fe^{2+}$) was used to reach the conclusion.

In this work we use the extended x-ray absorption fine structure technique (EXAFS) to probe the microscopic structure around the Fe site. This technique allows one, in principle, to determine the distances, numbers, and identities of the atoms in the first few coordination shells of Fe. In practice, it is at present difficult to distinguish between oxygen and nitrogen ligands and the error in the determination of the absolute number of ligands even in the first coordination shell is ~10–20%, which renders it difficult to

distinguish, for instance, between five and six ligands. This error is considerably smaller when one compares nearly identical compounds. This is the case in the present work in which EXAFS spectra from reaction centers having two, one, and zero quinones (2Q, 1Q, 0Q) were compared. In addition, reaction centers with and without the electron transfer inhibitor *o*-phenantroline were compared to determine whether this electron inhibitor binds to Fe. The EXAFS spectra obtained from the reaction centers were compared with those obtained from several model compounds having different numbers of O, N, C, and S, bound to Fe. A preliminary account of this work has been presented earlier (Eisenberger et al., 1980).

THE EXAFS TECHNIQUE

Basic Principles

The EXAFS technique has been thoroughly reviewed by numerous authors (Stern, 1978; Eisenberger and Kincaid, 1978; Winick and Doniach, 1980; Cramer and Hodgson, 1979; Lee et al., 1981), with several of the reviews specifically dealing with applications to molecules of biological interest (Shulman et al., 1978*a*; Chan and Gamble, 1978; Doniach et al., 1980).

The technique involves the accurate measurement of the x-ray absorption coefficient of a sample in an energy region where the atom of interest (in our case, iron) has an absorption threshold of its deeply bound electrons (7,120 eV). Such a measurement is shown in Fig. 1. Note the threshold near 7,120 eV and the oscillations above this energy. These oscillations constitute the desired EXAFS signal. They arise when the incident photon has an energy, E, that is greater than the binding (threshold) energy, E_0. The energy of the photoelectron E_{elec} is given by

$$E_{elec} = E - E_o = \frac{\hbar^2 k^2}{2m}, \quad (1)$$

where k is the wave vector $2\pi/\lambda_e$ of the photoelectron whose wavelength is λ_e.

The emitted photoelectron can scatter from the neighboring atoms; this process depends on the distance R_{ij} that separates the absorbing atom i from the scattering atom j. The strength of the scattering depends on the number of scattering atoms, N_j at a distance R_{ij}, as well as on the atomic number of the scattering atoms j. The scattered electron wave and the original outgoing wave can interfere at the original absorbing site in a way that modulates the strength of atomic absorption μ_A to result in the total absorption, μ_T, as shown in Fig. 1. An expression for the normalized extra contribution caused by this process for the case of a gaussian distribution of distances R_{ij} (owing to either thermal or static disorder) is given by

$$\chi_i = \frac{\mu_T(E) - \mu_A(E)}{\mu_A(E)} = \sum_j \frac{N_j}{kR_{ij}^2} |f_j(k,\pi)| e^{-2k^2\sigma_j^2} e^{-2R_{ij}/\lambda} \{\sin [2kR_{ij} + \psi_{ij}(k)]\}, \quad (2)$$

where $f_j(k,\pi)$ is the strength of the scattering process and varies from one atom to another, $e^{-2R_{ij}/\lambda}$ describes the attenuation of the electron as it travels from the absorbing atom with a mean free path λ to the scattering atom and back, and $\psi_{ij}(k)$ is the phase shift that the electron experiences. Thus, from the frequency of the oscillation one can determine the distances if ψ_{ij} is known. The amplitude can be used to determine N_j and the chemical identity of the scatterer if σ_{ij} and λ can be properly taken into account. In general, ψ_{ij} can be obtained accurately enough to determine distances with an accuracy of $\pm(0.01 - 0.02)$ Å (Lee and Beni, 1977; Citrin et al., 1976). The amplitudes are more difficult to determine accurately, so that coordination numbers can usually be determined only to $\sim\pm(10\text{–}20)\%$ (Stern et al., 1980; Eisenberger and Lengeler, 1980). One can in many cases distinguish elements in different rows and in some cases elements within the same row (Reed et al., 1977) of the periodic table.

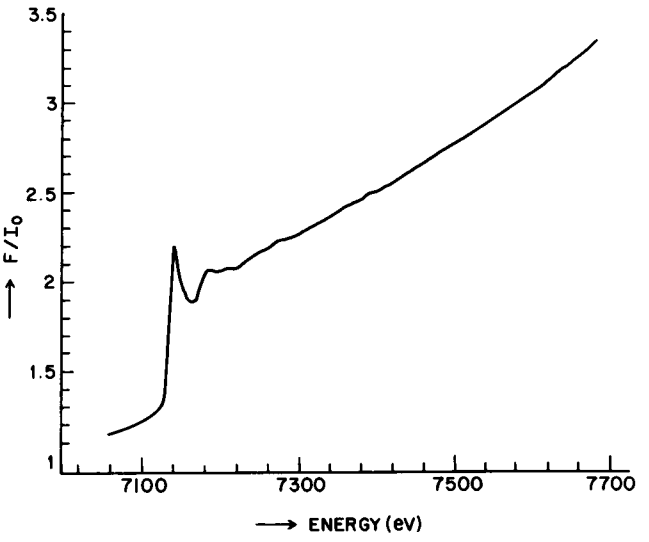

FIGURE 1 X-ray absorption spectrum of Fe^{2+} in reaction centers with two quinones (T = 130°K). F is the fluorescence intensity and I_0 is the intensity of the incident beam.

Data Analysis

The unprocessed EXAFS data for the 2Q sample are shown in Fig. 1. To extract from this simple curve all the parameters of Eq. 2 (i.e., N_j, R_{ij}, ψ_{ij}, σ_{ij}, λ, $f[k,\pi]$) is a formidable and often impossible task. Fortunately, we are mainly interested in comparing N_j and R_{ij} between samples, which facilitates the analysis considerably.

The first step in the analysis is to isolate the oscillating part $\chi(k) = [\mu_T(E)] - \mu_A(E)]/\mu_A(E)$. After removing the slope of the spectrum by a simple straight-line subtraction routine (Fig. 2 *a*), the value of the edge jump $\mu_A(E_0)$ is determined from the difference in the heights of the straight line fits below and above the edge (Fig. 2 *a*). We obtained the difference between the oscillating EXAFS part and the smooth atomic part by a spline background removal routine (de Boor, 1968; Fox et al., 1976), taking into account the k-dependence of $\mu_A(E)$. We used the position of the first peak as the threshold energy E_0 (Eq. 1) to determine the value of k at each energy (see arrow in Fig. 2 *a*). The result of this procedure is shown in Fig. 2 *b*, where $\psi(k)$ has been multiplied by k^2 to weight the EXAFS oscillations more uniformly[1] over the range of k-values of interest, i.e., in our case $3 < k < 8$ Å^{-1}.

Next, a complex Fourier transform is performed on $k^2\chi(k)$. We Fourier transformed $k^2\chi(k)$ between 0 and 10 Å^{-1}, although only data between 3 and 8 Å^{-1} were used to extract structural information. The alternate procedure of Fourier transforming between 3 and 8 Å^{-1} is likely to introduce termination errors and was, therefore, not used. The magni-

[1]An alternate choice that is often made is to multiply $\chi(k)$ by k^3. Although the shape of the curves depends on the particular choice, the results do not depend on it.

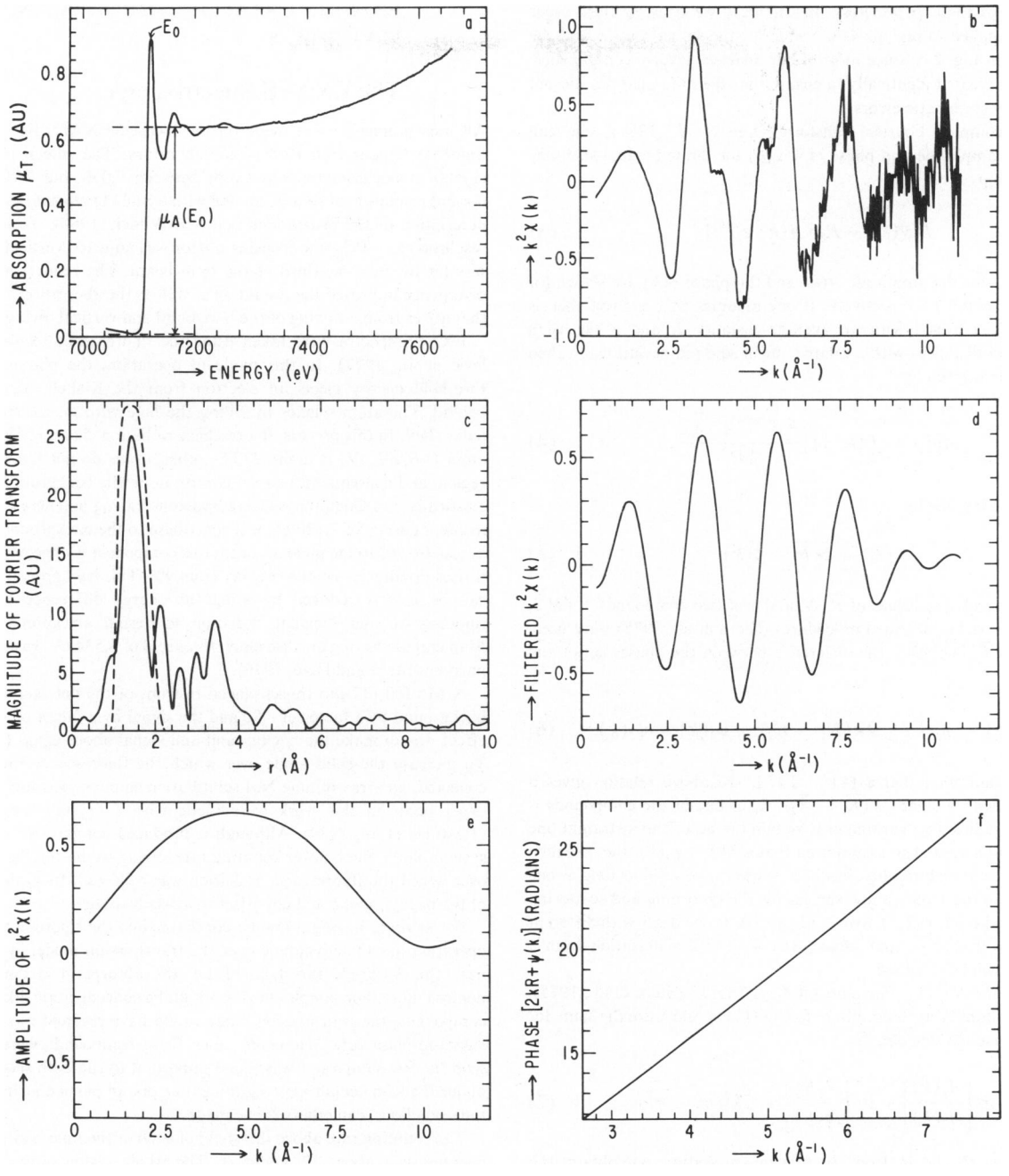

FIGURE 2 Processing of EXAFS data of reaction center sample with two quinones (see Fig. 1). (*a*) After removal of background slope of Fig. 1. (*b*) Oscillating EXAFS part multiplied by k^2. (*c*) Magnitude of Fourier transform of (*b*) between $0 < k < 10$ Å^{-1}. The dotted line is the filtering window used to isolate the first coordination shell. (*d*) Filtered $k^2\chi$ of the first coordination shell obtained by backtransforming (*c*). (*e*) The magnitude of the amplitude function $A(k)$ of (*d*). (*f*) The phase $\phi(k)$ of (*d*). AU, arbitrary units.

tude of the Fourier transform is shown in Fig. 2 *c*. The contributions of the different shells of neighbor atoms are clearly discernible, although it must be kept in mind that because of the phase factor ψ_{ij} (Eq. 2), distances cannot be read off directly.[2] By selectively placing a smooth filter (window) (Hayes et al., 1976; Eisenberger and Kincaid, 1978) around one of the peaks (see dotted line in Fig. 2 *c*), a particular coordination shell can be isolated and backtransformed into *k*-space (Fig. 2 *d*). The smoothness of the curve, as compared with Fig. 2 *b*, is due to the filtering of the high-frequency noise by the window. Care was taken that the spline fit to the background and the Fourier filtering produced no distortion of the structural information. The lack of distortion was verified by varying the order of the spline removal and the width of the Fourier filter and establishing a region in which the result was essentially

[2]For Fe—O and Fe—N, ~0.5 Å has to be added to the distances read off Fig. 1 *d*. The precise value is determined by the procedure outlined in the text.

independent of these parameters. In this case we chose a third-order polynomial applied to regions 4-Å^{-1} wide for the spline routine and the filter shown in Fig. 2 *c*. Since most of our analyses involve comparisons, all data were treated identically to ensure that the data analyses did not introduce any systematic errors.

Using a complex Fourier transform (Lee et al., 1981), one can generate the amplitude and phase of $k^2\chi(k)$ for the individual shells by the relationship

$$k^2\chi(k) = Re[A(k)\, e^{i\phi(k)}]. \tag{3}$$

The results for the amplitude $A(k)$ and the phase $\phi(k)$ are shown for 2Q in Fig. 2 *e* and *f*, respectively. If one assumes that a given shell is composed of N atoms with an average distance $\bar{R}$ and a Gaussian distribution of distances with a relative mean squared deviation, σ^2, then the amplitude is given by

$$A(k) = |f(k, \pi)| \frac{Ne^{-2k^2\sigma^2}e^{-2\bar{R}/\lambda}}{k\bar{R}^2}, \tag{4}$$

and the phase is given by

$$\phi(k) = 2k\bar{R} + \psi(k). \tag{5}$$

To obtain the relative values of $\bar{R}$, N, and σ of two compounds 1 and 2, the following well established procedures (Stern et al., 1975) were used: to determine $\bar{R}$, one takes the difference between the phases $\phi_1(k)$ and $\phi_2(k)$:

$$\phi_1(k) - \phi_2(k) = 2k(\bar{R}_1 - \bar{R}_2) + \psi_1(k) - \psi_2(k). \tag{6}$$

On the assumption that $\psi_1(k) = \psi_2(k)$, the above relation gives a straight line with a slope $2k(\bar{R}_1 - \bar{R}_2)$. E_0 of one of the compounds is treated as an adjustable parameter to obtain the best fit to a straight line passing through zero. The assumption that $\psi_1(k) = \psi_2(k)$, the so-called chemical phase transferability, has been shown to be valid as long as one is dealing with the same atomic species for the absorbing and scattering atom (Lee and Beni, 1977; Citrin et al., 1976). If one deals with different ligands, E_0 will change; and since $\psi_1(k) \neq \psi_2(k)$, a deviation from a straight line will be obtained.

To determine N and σ, one plots $\ln(A_1/A_2)$ vs. k^2 (Stern et al., 1975). Making the simplifying assumption that $|f(k,\pi)|$ and λ are the same for the two compounds, one obtains

$$\ln\left[\frac{A_1(k)}{A_2(k)}\right] = \ln\left[\frac{N_1R_2^2}{N_2R_2^2}\right] + 2k^2(\sigma_2^2 - \sigma_1^2). \tag{7}$$

Thus, knowing R_1 and R_2 from the previous procedure, one obtains the ratio N_1/N_2 from the intercept at $k = 0$ and the quantity $2(\sigma_2^2 - \sigma_1^2)$ from the slope. The mean squared deviation σ^2 can arise either from a static disorder of the ligands or from a dynamic effect, i.e., lattice vibrations. When the differences in ligand distances within a coordination shell of the absorbing atom are small ($\Delta R < 0.1$ Å), the functional dependence of the amplitude decay is similar to that obtained from thermal disorder (Shulman et al., 1978*b*). However, for differences so large that $(\Delta R)k$ becomes a significant fraction of a radian, interference effects will cause beats in the amplitude function $A(k)$, and hence Eq. 7 will not be applicable. The assumption that $|f(k,\pi)|$ and λ are the same for both compounds is likely to be justified for all reaction center samples, but it may not hold for many of the model compounds. In general, amplitude transferability between different compounds is not as good a concept as chemical phase transferability discussed earlier. It is desirable, therefore, to investigate as many model compounds as possible, preferably in classes each of which has several compounds with the same type of ligands.

EXPERIMENTAL TECHNIQUES AND MATERIALS

The EXAFS Spectrometer

All measurements were made on the focused EXAFS line II-3 at the Stanford Synchrotron Radiation Laboratory. The silicon (111) Bragg crystal monochromator was swept between 7,050 and 7,700 eV. The normal resolution of that beam line with a Si(111) crystal is ~8 eV (for a description of the instrumentation, see Winick, 1980). To increase the resolution to ~3 eV, the focusing mirror was adjusted vertically so that it was hit by only one-third of the total beam. The reduction in vertical divergence improved the resolution as well as the aberration of the mirror that arises from a mixing of the horizontal and vertical divergences.

EXAFS spectra were taken using the fluorescence techniques (Jaklevic et al., 1977). In this mode of operation, the photon above the threshold energy ejects an electron from the K-shell, leaving a hole behind. The atom relaxes by filling the hole with an electron from an outer shell. In this process, fluorescence radiation characteristic of the Fe atom (~6,400 eV) is emitted. The other atoms do not fluoresce in this region, and consequently do not contribute to the background. However, elastically and Compton scattered photons having an energy close to the incident energy of 7,120 eV will contribute to the background. Although at exactly 90° to the incident beam this component is expected to be zero, it rises rapidly as one moves away from 90°. This background component can be greatly reduced by using the energy difference between the fluorescence and incident radiation to design an appropriate filter. Managanese having an absorption threshold of 6,534 eV was used for this purpose (Stern and Held, 1979).

A Mn foil (17-μm thick) placed in front of the detector reduced the background by a factor of ~50 and the signal by a factor of ~2. The net effect was to make the background and signal about equal (see Fig. 1). To increase the solid angle over which the fluorescence radiation was collected, an array of nine NaI scintillation counters was used. The early experiments in this work were made with a crystal monochromator (Hastings et al., 1979). Although it produced comparable results, that system had a much lower counting rate, owing to the smaller solid angle over which the fluorescence radiation was collected. Its higher rejection of the background could not offset this disadvantage.

For samples having a low Fe concentration, the fluorescence mode of operation has the advantage over the transmission mode, in which even near the 7,120-eV threshold of Fe, the absorption is dominated by noniron atom. For samples having a high Fe concentration, like the model compounds, the transmission mode would have resulted in an improved signal-to-noise ratio. However, since these compounds were compared with the RC samples, it was found important to run both sets of samples under the same conditions; significant errors, in particular in the amplitude functions, can otherwise be made.

The counting rate above threshold of each of the nine NaI scintillation counters was about 10^5 counts/s. The whole system was shown to be linear to better than 10%. The scanning was done by a stepping motor in energy steps of 1.5 eV. Typically, the total scanning time over an energy range of 600 eV was ~10 min. The total counts of the fluorescence radiation at each energy were divided by a monitor signal that was proportional to the incident beam intensity at that energy. The monitor signal was obtained by an ionization chamber located in the beam between the monochromator and the sample (Winick, 1980). Multiple scans were run on each sample. For RC, the number of scans per sample varied between 10 and 25; for the model compounds fewer scans were needed.

Most RC samples were run at cryogenic temperatures. The Dewar, constructed for this purpose, was designed from lucite lined with styrofoam. (Preliminary experiments showed that blue styrofoam gave a strong Fe background; replacements with white styrofoam eliminated the problem.) The window for the beam entry was made by evacuating the space between two 0.0015-in. silvered mylar sheets (Transilwrap West

Corp., Downey, Calif.). The sample could be inserted and removed from the Dewar at low temperatures. A copper-constantan thermocouple in thermal contact with the rexolite sample holder was used to monitor the temperature. By varying the flow of cold nitrogen into the Dewar, the sample temperature could be varied between 80°K and room temperature. A convenient temperature at which most of the experiments with RC were performed was 130°K.

Reaction Center Samples

Reaction centers from *R. sphaeroides* R-26 were purified as previously described (Feher and Okamura, 1978). Two independently prepared sets of samples containing ~2, 1, and 0 quinones/RC were prepared by the method of Okamura et al. (1975). The quinone and iron contents were determined as described in part I of this work (Butler et al., 1980). All samples were found to contain <0.03 heme/RC.

To maximize the signal-to-noise ratio of the EXAFS signal, the highest attainable protein (i.e., Fe) concentration is desired. To this end RC were embedded in polyvinyl alcohol (PVA), which also offers the additional advantage of stability[3] and ease of handling. 1 ml of a 10% wt/vol PVA (88% hydrolyzed average mol wt = 125.000, Aldrich Chemical Co., Inc., Milwaukee, Wis.) solution in TL buffer (0.025% LDAO, 10 mM Tris-Cl, pH8) was mixed with 3 ml of RC in TL buffer having an absorbance of $A_{1\,cm}^{800} \simeq 100$. In one set of samples two times excess (over Fe) of *o*-phenantroline was added. The PVA-RC solution was poured into a Teflon trough and evaporated in the dark by blowing dry nitrogen through an inverted funnel over it. The dry film had a thickness of ~0.1 mm and an optical absorbance at 648 mm of 1.2, corresponding to an absorbance of ~15 at 800 nm. This corresponds to a ~5 mM (~50% wt/vol) protein concentration (i.e., ~3 × 10^{18} Fe/cm^3). The film was peeled off and 11 mm × 5 mm samples were punched out with a beryllium-copper die. Ten of these were sandwiched together to make one EXAFS sample.

A different set of samples was made by first concentrating RC in an Amicon M-3 cell (Butler et al., 1980) to a concentration of ~1 mM (A_{1cm}^{800} = 300) (Amicon Corp., Scientific Sys. Div., Lexington, Mass.). An additional factor of two in concentration was obtained by placing the sample on an Amicon membrane on top of a filter paper (Whatman No. 1, Whatman, Inc., Clifton, N.J.). The final solution had the consistency of a paste with an absorbance (determined by dilution) of $A_{1cm}^{800} \simeq 600$, corresponding to a 2-mM protein concentration. Reduced samples were prepared by replacing LDAO with Triton X-100, adding sodium dithionite anaerobically, and freezing at 77°K (Butler et al., 1980). Samples containing two times excess of *o*-phenantroline were also prepared. The quinone and Fe contents of the RC samples that were analyzed by EXAFS are shown in Table I.

A special set of samples was made to study possible radiation damage effects of the RC samples. RC were embedded in PVA (see above) to obtain a final optical absorbance $A^{800} \simeq 1.5$ for optical measurements and $A^{800} \simeq 3$ for EPR investigations. The samples were cut into strips that approximated the size of the beam (6 × 2 mm). To align the beam, a sample with an Fe foil backing was translated in a plane perpendicular to the beam direction until the maximum count rate at the detector was obtained. EPR and optical spectra and the kinetics of bleaching and recovery were obtained as previously described (McElroy et al., 1974).

Model Compounds

The model compounds used in this work are summarized in Table II. Compounds Nos. 1, 4, 5, 6, and 9 were kindly supplied by A. W. Addison, (Drexel University) No. 8 by D. N. Hendrickson (University of Illinois), and No. 10 by W. W. Parson (University of Washington). Compounds Nos. 11, 12, and 13 were purchased from Alfa Div., (Ventron Corp., Danver, Mass.), and Nos. 2 and 3 from Sigma Chemical Co., St. Louis, Mo. (type III). Compounds Nos. 1, 4–12 came in powdered form. They were diluted with ultrapure sucrose (Schwarz/Mann Div., Becton, Dickinson & Co., Orangeburg, N.Y.) to a concentration of ~10 mM. To avoid geometric resonance effects in the x-ray absorption coefficient, both the sucrose and the compounds were ground to a fine powder before mixing. The dimensions of the samples were the same as those of the RC samples. They were placed into rexolite slabs having the appropriate shape (11 mm × 5 mm × 2 mm), milled out and covered with 0.001-inch Mylar tape. Cytochrome *c* (horse heart) (cyt *c*) was oxidized and reduced as described previously (Rosen et al., 1980) and embedded in PVA to a final concentration of 10 mM. Similarly, solutions of potassium ferricyanide (No. 13) were mixed with PVA to give films having Fe concentrations of 2, 4, 8, and 16 mM. These samples were used to optimize the spectrometer settings and to test its linearity. In addition to the above samples, a control PVA sample having only TL buffer was prepared.

TABLE I
REACTION CENTER SAMPLES

No.	Sample	Q/RC‡	Fe^{2+}/RC‡	Solvent and buffer
1	2Q	1.94 ± 0.05	1.00 ± 0.02	PVA + TL§
2	1Q	1.02 ± 0.05	0.94 ± 0.02	PVA + TL
3	0Q	0.08 ± 0.02	1.11 ± 0.02	PVA + TL
4	2Q*‖	2.00 ± 0.05	0.91 ± 0.02	PVA + TL
5	1Q*	1.05 ± 0.05	0.90 ± 0.02	PVA + TL
6	0Q*	0.08 ± 0.02	1.03 ± 0.02	PVA + TL
7	2Q* + *o*-phen.	2.00 ± 0.05	0.91 ± 0.02	PVA + TL
8	1Q* + *o*-phen.	1.05 ± 0.05	0.90 ± 0.02	PVA + TL
9	0Q* + *o*-phen.	0.08 ± 0.02	1.03 ± 0.02	PVA + TL
10	1Q* red	1.05 ± 0.05	0.90 ± 0.02	TT¶
11	2Q* aqueous	2.00 ± 0.05	0.91 ± 0.02	TL

Quoted errors represent one standard deviation of the mean.
‡The ubiquinone and iron concentrations were measured before embedding the RC in PVA.
§TL buffer: 10 mM Tris-Cl, pH 8, 0.025% LDAO. Concentrations after mixing RC with PVA (but before drying process).
‖All starred samples (*n*Q*) came from the same original preparation of RC; the three unstarred samples also came from one, but from a different preparation.
¶TT buffer: 10 mM Tris-Cl, pH 8, 0.1% Triton X-100.

EXPERIMENTAL RESULTS

Comparison of RC Samples with Different Numbers of Quinones

The First Coordination Shell. EXAFS spectra of the first coordination shell from samples having ~2, 1, and 0 quinones (2Q, 1Q, and 0Q of Table I) were obtained as described earlier (see Fig. 2 *c, d*). The result of the filtered $k^2\chi$ plots are shown in Fig. 3, where 1Q and 0Q are compared with the 2Q sample. The amplitudes can be seen to be approximately the same for the 2Q and 1Q spectra but different for the 2Q and 0Q spectra. By plotting the ln of the ratio of the amplitudes vs. k^2 (see Fig. 4 and Eq. 7) and extrapolating to $k = 0$, we obtained

$$\ln\left[\frac{A(2Q)}{A(1Q)}\right] = 0.02 \pm 0.03; \ln\left[\frac{A(2Q)}{A(0Q)}\right] = 0.12 \pm 0.06.$$

[3]Samples that were kept at 4°C for 2 yr showed no changes in their optical spectra. The kinetics of charge recombination of RC embedded in PVA were found to be the same as in aqueous samples.

TABLE II
MODEL COMPOUNDS

X No.	Compound	Ligand coordination, L	Spin* state	Ligand structure
1	$[Fe^{2+}L_3][BF_4]_2$	N_6	L.S.	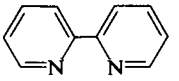
2	cyt c^{2+}	N_5S	L.S.	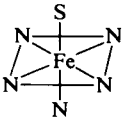
3	cyt c^{3+}	N_5S	L.S.	
4	$[Fe^{3+}L][BF_4]$	N_4O_2	L.S.	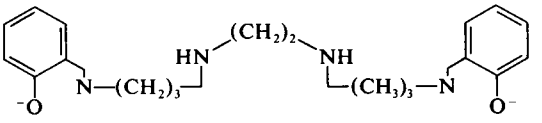
5	$[Fe^{3+}L]PF_6$	N_4O_2	H.S.	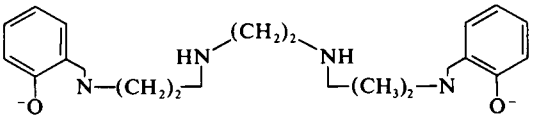
6	$[Fe^{3+}L_3]$	N_3O_3	H.S.	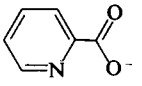
7	$[Fe^{3+}L]Na$	N_2O_4	H.S.	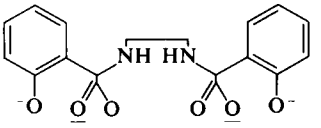
8	$[NaFe^{3+}L_2]$	N_2O_4	H.S.	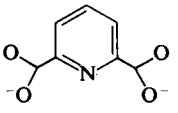
9	$[Fe^{3+}L]$ o-BQ$^-$	N_2O_4	H.S.	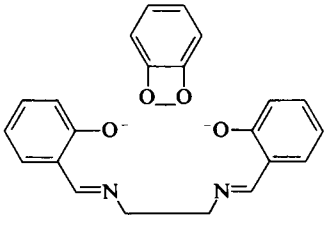
10	$Fe^{3+}L_3$ acetyl acetonate	O_6	H.S.	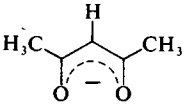
11	$Fe^{2+}L_2$	O_6	?	
12	$[Fe^{2+}L]—2H_2O$ oxalate	O_6	H.S.	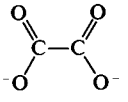
13	$Fe^{2+}(NH_4)_2SO_46H_2O$	O_6	H.S.	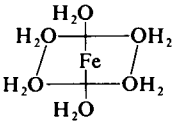
14	$K_3Fe^{3+}(CN)_6$ ferricyanide	C_6	L.S.	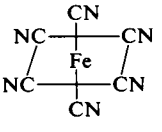
15	Bisimidazole proloheme IX-Fe^{3+}	N_6	L.S.	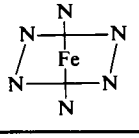

*L.S., low spin; H.S., high spin.

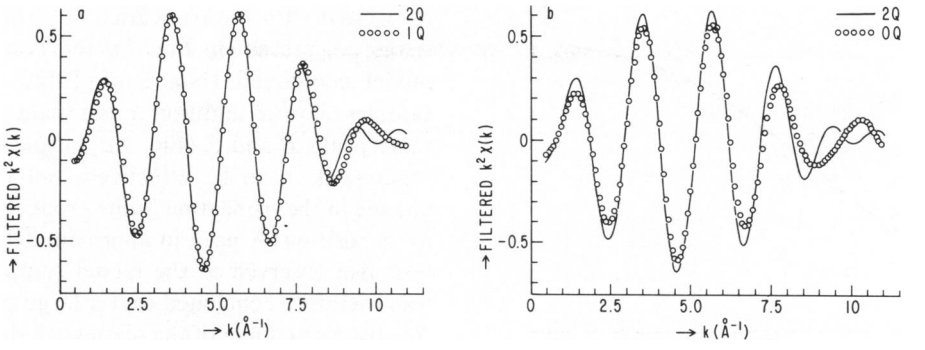

FIGURE 3 Comparison of filtered (first shell) $k^2\chi$ spectra of reaction centers with two and one quinones (*a*) and two and no quinones (*b*). Spectra taken at 130°K.

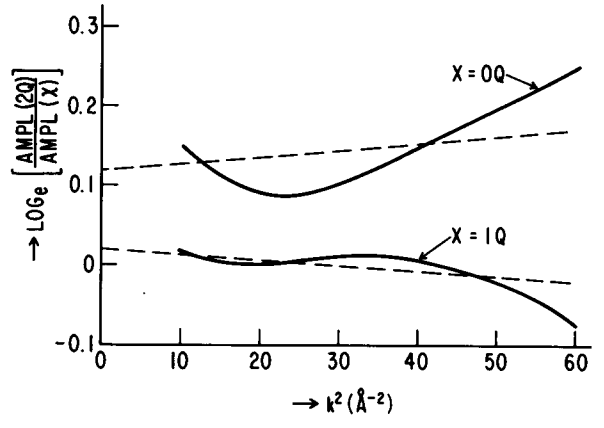

FIGURE 4 The ln of the ratio of the amplitude functions of the 2Q sample to that of the 1Q and 0Q samples vs. k^2 (solid line). The intercepts at $k = 0$ (dashed line) give the ratios of the coordination numbers (Eq. 7).

Thus, the amplitude of the 0Q sample is ~12% smaller than for the corresponding 2Q sample, which suggests a loss of one ligand. For this case, however, the ln amplitude-vs.-k^2 plot exhibited a large deviation from a straight line (Fig. 4). Such a behavior is expected from the interference effects caused by a large change in bond lengths or chemical identity of the Fe^{2+} ligands.

Similar results were obtained earlier on an independent set of samples (2Q*, 1Q*, 0Q* of Table I) with a crystal monochromator. However, as discussed above in Experimental Techniques, the signal-to-noise ratio of this system was lower than that obtained with the Mn filter; consequently, the errors in the amplitude determinations were larger than those quoted above. These results will be presented in the section dealing with the effect of *o*-phenanthroline.

The relative average distances of the ligands were obtained by plotting the phase differences (see Eq. 6 and Fig. 2*f*). From the slopes of these plots we obtained

$$\overline{R}(2Q) - \overline{R}(1Q) = 0.00 \pm 0.01 \text{ Å};$$

$$\overline{R}(2Q) - \overline{R}(0Q) = 0.02 \pm 0.01 \text{ Å}.$$

The difference spectra of 2Q and 0Q were analyzed for a possible missing ligand, i.e., $k^2\chi(0Q)$ was subtracted from $k^2\chi(2Q)$. The resultant $k^2\chi(2Q - 0Q)$ had a distance $\overline{R}$ that was 0.05 Å longer and an amplitude ~5 times smaller than that corresponding to 2Q.

The disorder parameter σ^2 arises from both static (structural) and dynamic (vibrational) disorders. The vibrational part can be determined from the temperature dependence of σ^2. For this purpose, EXAFS spectra of the 2Q sample were obtained at 130 and 300°K (Fig. 5). From the slope of the ln (amplitude)-vs.-k^2 plots (see dashed line of Fig. 6 and Eq. 7), we obtained

$$\sigma^2(300°K) - \sigma^2(130°K) = 0.0016 \pm 0.0003 \text{ Å}^2.$$

This value is significantly smaller than the values obtained by comparing the 2Q sample with "ordered" model compounds (to be discussed later). Thus, the disorder observed in the RC samples is predominantly static (structural) in nature.

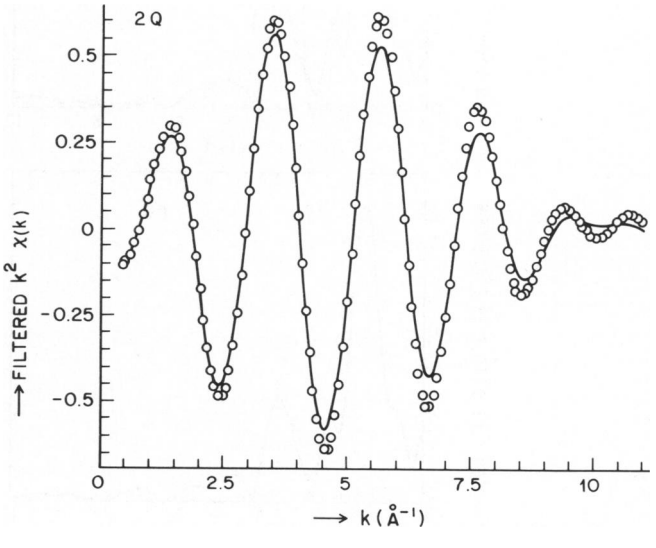

FIGURE 5 EXAFS spectra of RC sample 2Q taken at 300°K (solid line) and 130°K (open circles). From a comparison of the amplitudes the vibrational contribution to the disorder parameter was determined (see Eq. 7).

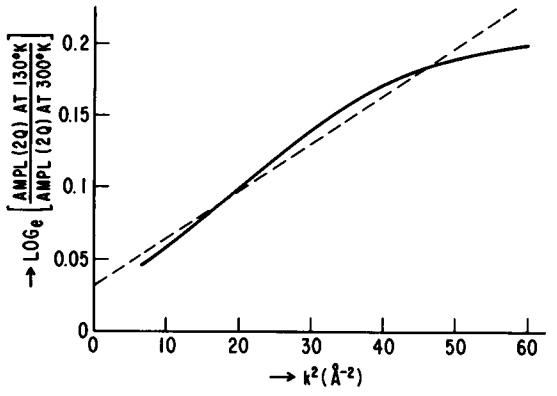

FIGURE 6 The ln of the ratio of the amplitude functions of the 2Q sample at 130 and 300°K vs. k^2 (solid line). From the slope the temperature dependent part of σ^2 was obtained (Eq. 7). Theoretically, the line should pass through zero; instead the observed intercept (dashed line) is at ~0.03. Thus, the minimum error in the determination of relative coordination numbers is ~3%.

Other Coordination Shells. The amplitudes of the Fourier transforms of $k^2\chi(k)$ are shown in Fig. 7. Since in this case we want to inspect the transform for significant features, the transform was performed in the range of meaningful EXAFS data, i.e., $3 < k < 8$ Å^{-1} (rather than $0 < k < 10$ Å^{-1}, as in Fig. 2 *c*, where the information was obtained from the backtransform 2*d*). To check whether some peaks arise from possible artifacts associated with the truncation and transformation procedures, we present in Fig. 7 *d* the Fourier transform of a model compound (No. 6 of Table II). All three RC samples show in addition to the main peak *A* at least two more peaks *B* and *C* (Fig. 7 *a*). Peak *B* is too close to the main peak *A* to be effectively isolated; furthermore, a change in the truncation limits produced a significant shift in its position. A peak in approximately the same position was also observed in the model compound (Fig. 7 *d*). It was therefore concluded that a large contribution to peak *B* is from side lobes of the main peak that are generated by the transform. The position of peak *C*, however, was not affected when the truncation limits were changed, and no peak at the equivalent position is present in the model compound. It thus corresponds to a more distant coordination shell.

The shell corresponding to peak *C* was isolated with an appropriate filtering window (see dotted line in Fig. 7 *a*) and analyzed in a manner analogous to the first coordination shell. The filtered $k^2\chi(k)$ functions are shown in Fig. 8 where 2Q is compared with 1Q and 0Q. Within the experimental accuracy (~10%), the amplitudes are approximately the same. Particularly noteworthy is a comparison at low k of Figs. 3 *b* and 8 *b*, which provides additional evidence that the 12% reduction in the amplitude of $k^2\chi(k)$ found for the first coordination shell of 0Q is real.

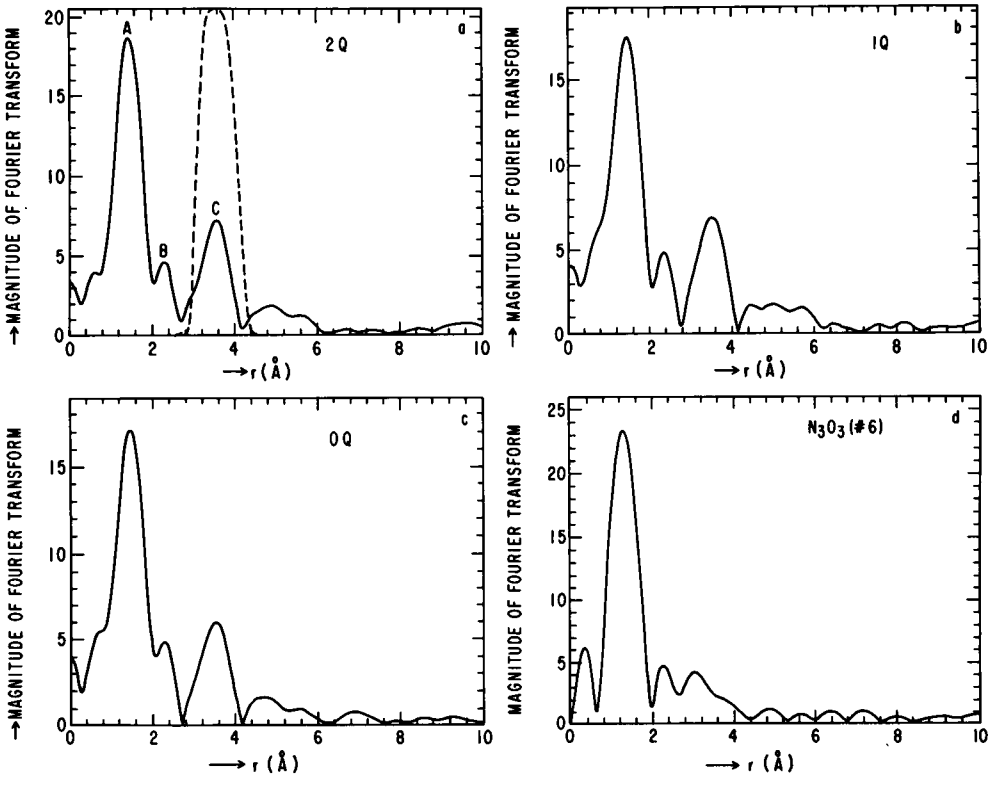

FIGURE 7 Magnitude of Fourier transforms of RC samples with two quinones (*a*), one quinone (*b*) and no quinones (*c*). The $k^2\chi(k)$ function was transformed between $3 < k < 8$ Å^{-1}. The more distant shell was isolated with the window function shown by the dotted line in (*a*). For comparisons, the Fourier transform of one of the model compounds (No. 6 of Table II) is shown in (*d*).

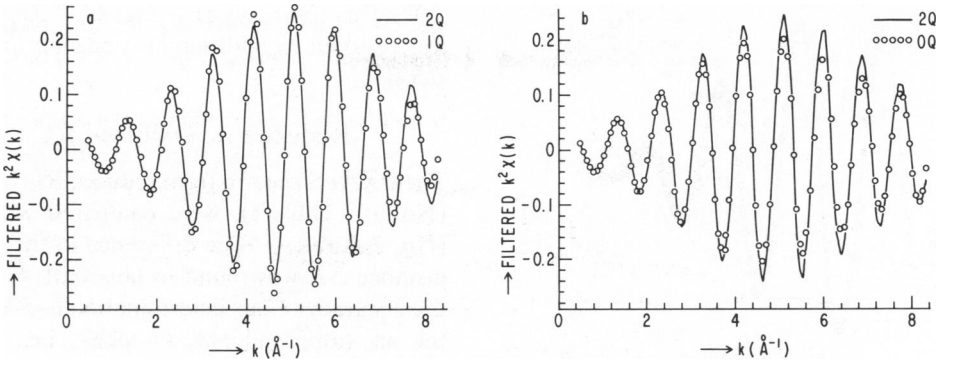

FIGURE 8 Comparison of filtered $k^2\chi(k)$ spectra from distant shell (see dotted line in Fig. 7 *a*) of reaction centers with two and one quinones (*a*) and two and no quinones (*b*). Spectra taken at 130°K.

The average distance of this shell was determined relative to the first coordination shell by plotting the phase difference of the two shells vs. k (Eq. 6). The result for the 2Q and 1Q samples was $\overline{R}(C) - \overline{R}(A) = 2.04 \pm 0.04$ Å. The difference in the disorder parameter σ^2 between 300 and 130°K for the 2Q sample was determined to be $\sigma^2(300°K) - \sigma^2(130°K) = 0.007 \pm 0.001$ Å^2. The above value is about 3 times larger than that found for the first coordination shell. A larger value is expected since the vibrational displacements of two atoms that are bonded to each other are much more correlated (i.e., they exhibit a smaller relative motion) than those of a pair of atoms that are farther apart (Beni and Platzman, 1976). In addition, librational (bending) modes also can contribute to σ^2 of distant atoms.

The Absorption Edge. Eq. 2 used to analyze EXAFS data does not apply to energies in the vicinity of the absorption edge. That region of the spectrum is sensitive to the density of states and charge distribution around the absorbing atom (Shulman et al., 1976; Kutzler et al., 1980). Absorption peaks that are observed several electron volts below the absorption edge arise from transitions from the 1s to bound (e.g., 4s, 4p, 3d) states. The oscillator strength of these transitions depends on the local symmetry of the absorbing atom. For instance, it has been shown by Shulman et al. (1976) that the absorption of the 1s → 3d transition increased sevenfold on going from an octahedrally to a tetrahedrally coordinated Fe site. Removal of a ligand could, therefore, change this absorption.

The absorption spectra near the edge are compared in Fig. 9 for the 2Q and 0Q samples. Although the relatively low resolution of the synchrotron, EXAFS II-3, line was not ideally suited for investigating the detailed features of the edge absorption, we can put limits and draw some conclusions from the observed results. A pre-edge absorption peak larger than ~3% of the absorption edge would have been observable with this system. For iron in a tetrahedral environment the peak height of the 1s-3d transition was found to be ~15% of the absorption edge (Shulman et al., 1976). The absence of such a peak in RC (at the approximate position shown by the arrow in Fig. 9) indicates that the iron site does not have tetrahedral symmetry, a conclusion that had been reached previously from other experiments (Butler et al., 1980; Boso et al., 1981). The position of the edge was found to be within ±2 eV for all three samples (2Q, 1Q, and 0Q).

The Effect of *o*-phenanthroline

To test whether *o*-phenanthroline, a known Fe chelator and electron transfer inhibitor, binds to Fe, EXAFS spectra were taken on samples containing excess *o*-phenanthroline. An analysis of the filtered $k^2\chi(k)$ spectra (Fig. 10 *a*) obtained on the 1Q sample with and without *o*-phenanthroline showed that there is no change in the amplitude, i.e., coordination number ($\Delta N/N < 5\%$) or average distance $\overline{R}$ ($\Delta R < 0.01$ Å).

An earlier set of experiments was performed with the crystal monochromator detection scheme on samples 2Q*, 1Q*, 0Q*, with and without *o*-phenanthroline (see Table I). This system had a poorer signal-to-noise ratio, so that there was greater uncertainty in the results. Within the experimental accuracy, however, the amplitudes of the first shell of 2Q* and 2Q* plus *o*-phenanthroline were found to be the same (Fig. 10 *b*). For comparison purposes

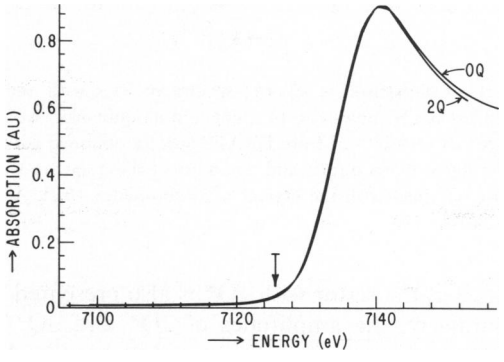

FIGURE 9 Comparison of the absorption edge of Fe^{2+} in reaction centers with two and no quinones. For tetrahedral iron, a 15% preabsorption peak (at the approximate position indicated by the arrow) was found by Shulman et al. (1976). No such peak is discernible in our data.

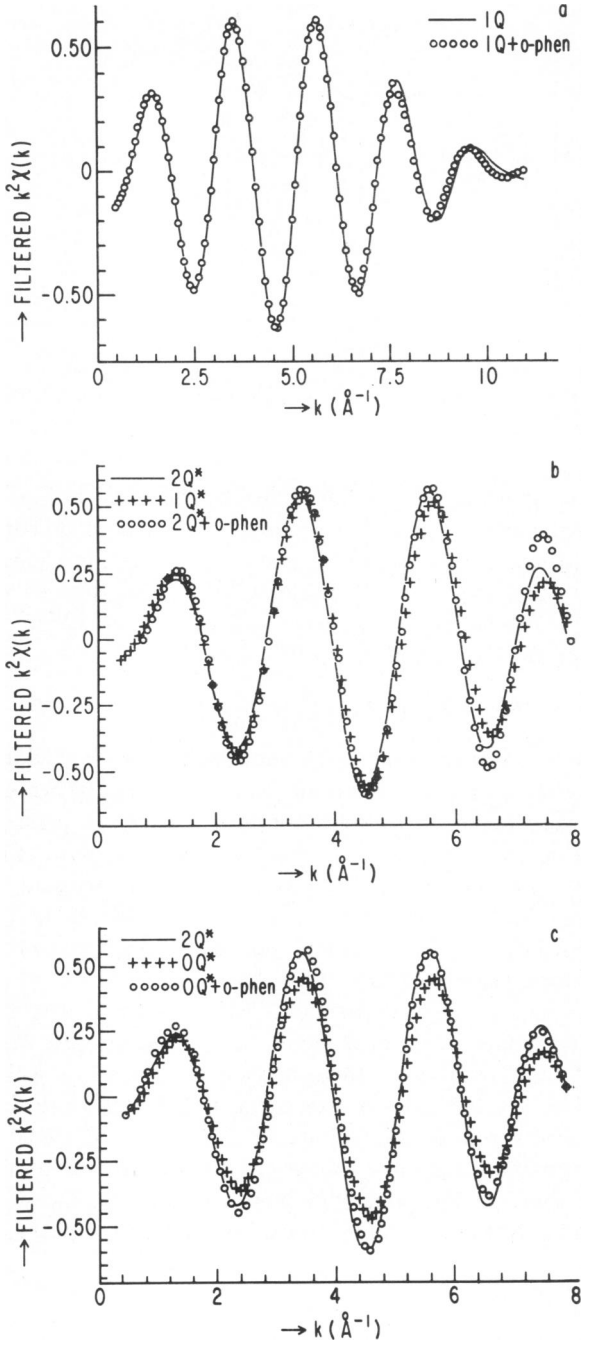

FIGURE 10 Comparison of $k^2\chi(k)$ spectra of RCs with and without *o*-phenanthroline. Samples had two, one and no quinones (see Table I). Top figure (*a*) was derived from EXAFS spectra obtained with the Mn filter. The signal to noise ratio and reliability of these spectra was higher than those obtained with the crystal monochromator (*b*,*c*). All spectra taken at 130°K.

with Fig. 3 *a*, the result with 1Q* is also presented in Fig. 10 *b*. Similarly, the amplitudes of 2Q* and 0Q* are in qualitative agreement with those presented in Fig. 3 *b*, i.e., the amplitude of 0Q* is smaller than that of 2Q*. Upon addition of *o*-phenanthroline to 0Q*, the EXAFS amplitude increases and becomes approximately equal to that of 2Q*. This result suggests that 0Q* had lost a ligand that was restored by addition of *o*-phenanthroline (see Discussion).

Reduced vs. Oxidized RC

The EXAFS spectra from reduced RC having one quinone (No. 10, Table I), were compared with unreduced RC (No. 2, Table I). The difference in the average first shell distance ΔR was found to be <0.01 Å. Similarly, within the accuracy of our determination (~5%), the intercept of the ln (amplitude)-vs.-k^2 plots, i.e., the coordination number did not change upon reduction. These results corroborate the earlier findings that Fe^{2+} does not change its valence when RC are reduced (Debrunner et al., 1975; Butler et al., 1980).

Comparison of RC with Model Compounds

So far we have discussed only the relative amplitudes, phases, and distances of the different RC samples. To determine their absolute values one needs to compare these parameters with those obtained from model compounds. We shall demonstrate the procedure that we used with a typical example, choosing acetylacetonate as a model compound with six oxygens liganded to Fe^{3+} (No. 10 of Table II) and comparing with to the 2Q sample (No. 1 of Table I).

The total phase $\phi(k)$ for the two samples is shown in Fig. 11 *a* and the phase difference $\Delta\phi(k)$ (together with another model compound) in Fig. 11 *b*. If the model compound had the same ligands and electronic charge distribution as the unknown (i.e., RC) sample, $\psi_1(k)$ would be equal to $\psi_2(k)$, and a straight line passing through zero would be obtained (Eq. 6). This is usually not the case (see full lines in Fig. 11 *b*). To deal with this problem, the computer program that was used searches for the best fit to a straight line passing through zero by varying E_0 of the model compound. The result is shown by the dashed lines in Fig. 9 *b*. For acetylacetonate (No. 10) the shift in E_0 was only 2 eV, and hence the difference between the dashed and full line is not very large. For ferricyanide, the shift in E_0 was ~10 eV, resulting in a significant change in the phase function. The value of the shift of E_0 serves as a guide to determine the similarity between the model compound and the RC sample. E_0 was determined for all model compounds and is summarized in Table III. From the slopes of the lines $\Delta\phi/\Delta k$ the differences in distance $\overline{R}(2Q) - \overline{R}(X)$ were obtained (Table III). To obtain the absolute values of $\overline{R}$ of the RC samples, the distances $R(X)$ of the model compounds must be known. Unfortunately, most of these have not yet been determined. The distances of five of them having C_6, N_6, O_6 ligands are known from x-ray crystallographic studies and were used to determine $R(2Q)$ (see Table IV). Note that the values of $R(2Q)$ obtained are rather insensitive with respect to these three low Z ligands.

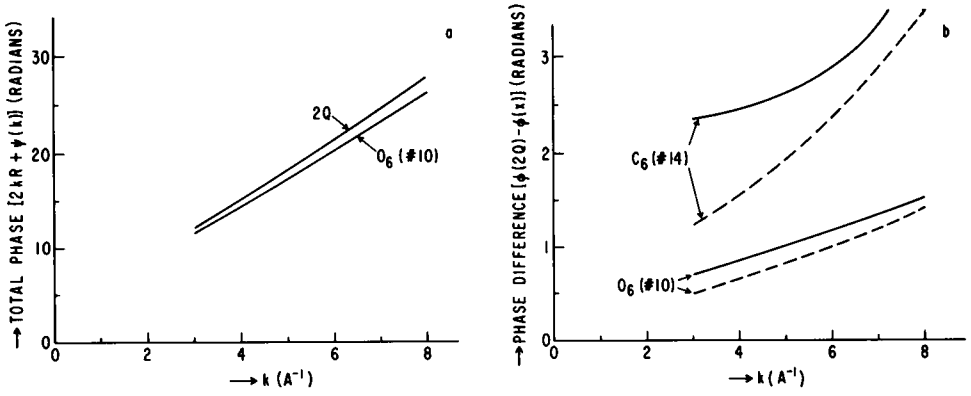

FIGURE 11 Comparison of phases of RC sample having two quinones (2Q) with those obtained from model compounds. (*a*) Total phase shift $\phi(k)$ of 2Q and acetylacetonate Fe^{3+}. (*b*) The phase difference, $\Delta\phi$, between 2Q and two model compounds. Numbers in parentheses identify the compounds (Table II). Solid lines were obtained by using E_0 as defined in Fig. 2 *a*. Dashed lines were obtained by varying E_0 of model compound for a best straight line fit passing through zero. The shifts in E_0 are summarized for all model compounds in Table III.

To determine the coordination number of the first shell the ln of the ratio of amplitudes of the RC sample to that of the model compound was plotted vs. k^2 and the intercept at $k = 0$ determined (see Eq. 7). This is shown in Fig. 12 for three compounds (Nos. 7, 8, and 9 of Table II), all of which have Fe^{3+} bound as a ligand to N_2O_4. Similarly, the intercepts at $k = 0$ for the other model compounds were determined and are summarized in Table III. When the deviation from a straight line is severe, it becomes difficult (and not meaningful) to fit the data to a straight line and the method of analysis is not applicable (see entries N.A., S (for straight), and C (for curved) in Table III). For example, in the case of Fe^{2+} oxalate an *S*-shaped curve with only a short straight section in the narrow range of $20 < k^2 < 40$ Å^{-2} (i.e., $4 < k < 6.3$ Å^{-1}) was obtained. Consequently, this seems to be a poor model compound from which to infer the coordination number.

The coordination numbers cannot be obtained from the intercept at $k = 0$ unless the k dependencies of $|f(k, \pi)|$ and λ are known. If the model compound and the unknown have the same ligands, $|f(k, \pi)|$ and λ are the same for both, and Eq. 7 can be used to evaluate the ratio of

TABLE III
COMPARISON OF EXAFS PARAMETERS OF RC WITH MODEL COMPOUNDS

X	Ligand*	$E_0(2Q) - E_0(X)$‡	$R(2Q) - R(X)$§	Intercept at $k = 0$ $\ln\left[\frac{\text{Amp}(2Q)}{\text{Amp}(X)}\right]$		$\frac{N(2Q)}{N(X)}$‖	½ slope of $\ln\left[\frac{\text{Amp}(2Q)}{\text{Amp}(X)}\right]$ vs. $k^2 \propto [\sigma^2(2Q) - \sigma^2(X)]$
(No.)		*(eV)*	*(Å)*				
1	N_6	10.1	0.109	0.20	C	1.35	0.007
2	N_5S	5.5	0.115	−0.15	C	0.96	0.005
3	N_5S	5.5	0.115	−0.08	S	1.03	0.006
4	N_4O_2	−5.0	0.186	0.10	C	1.33	0.009
5	N_4O_2	−2.8	0.164	(−0.10)	N.A.¶	N.A.	N.A.
6	N_3O_3	−1.6	0.097	0.01	S	1.09	0.004
7	N_2O_4	−2.5	0.108	0.07	C	1.19	0.002
8	N_2O_4	1.6	0.074	−0.07	S	1.00	0.007
9	N_2O_4	−2.2	0.105	−0.02	S	1.09	0.004
10	O_6	2.5	0.090	−0.10	S	0.99	0.010
11	O_6**	3.0	0.093**	−0.09	S	1.00	0.002
12	O_6	5.3	−0.021	(−0.40)	N.A.¶	N.A.	N.A.
13	O_6	2.0	−0.010	(−0.40)	N.A.¶	N.A.	N.A.
14	C_6	9.9	0.203	(−0.37)	N.A.¶	N.A.	N.A.
15	N_6‡‡	4.0	0.106	N.D.‡‡		N.D.	N.D.

*The ligand structure of these compounds is shown in Table II.
‡$E_0(X)$ adjusted for best-fit straight line passing through zero (see Fig. 11).
§Obtained from slope of $\Delta\phi$ vs. k plots (Fig. 11).
‖Calculated from the intercept at $k = 0$ and Eq. 7, taking for $R(2Q) = 2.10$ Å.
¶Obtained from plots like those shown in Fig. 12. S, straight line; C, curved line; N.A., severe deviation from a straight line which makes Eq. 7 not applicable for this case. A rough estimate is shown in parentheses.
**Since Fe^{2+} is expected to have a ligand distance ~0.1 Å larger than Fe^{3+}, one may suspect that this compound was inadvertently oxidized.
‡‡This compound had been run previously under different conditions (Shulman et al., 1978) and the amplitude could, therefore, not be compared with 2Q. (N.D., not determined).

TABLE IV

AVERAGE DISTANCE OF FIRST COORDINATION SHELL OF FE IN RCS FROM COMPARISON WITH MODEL COMPOUNDS

No.*	Model compound	Ligand	$\bar{R}$ of model compound‡	$\bar{R}$ of Reaction centers with 2 quinones§
			Å	
13	Potassium ferricyanide	C_6	1.903 ± 0.013‖	2.11
14	Bisimidazole protoporphyrin IX-Fe^{3+}	N_6	1.984 ± 0.013¶	2.09
10	Fe^{3+}-acetylacetonate	O_6	1.992 ± 0.006**	2.08
12	Fe^{2+}-oxalate	O_6	2.117 ± 0.033‡‡	2.10
13	Fe^{2+}-ammonium sulfate hexahydrate	O_6	2.126 ± 0.029§§	2.12

*Numbers refer to Tables II and III.

‡Errors represent the root mean square deviation of the ligand distances from R average.

§Obtained from R(2Q) − R(X), as listed in Table III.

‖Individual Rs are: two each 1.92, 1.90, 1.89 Å (Figgis et al., 1969).

¶Individual Rs are: 1.957, 1.980, 1.987, 1.990, 1.991, 1.999 Å (Collins et al., 1972).

**Individual Rs are: 1.986, 1.987, two 1.991, 1.993, and 2.004 Å (Iball et al., 1967).

‡‡Four carboxyls at 2.14 Å and two water molecules at 2.07 Å (Wyckoff, 1963).

§§Individual Rs are: two each 2.156, 2.136, 2.086 Å (Montgomery et al., 1967).

coordination numbers $N(2Q)/N(X)$. Since we lack information on the ligands of the RC sample, we were forced to make the simplifying assumption that $|f(k, \pi)|$ and λ are equal. (However, this assumption clearly cannot apply to all model compounds.) The values of $N(2Q)/N(X)$ obtained with this assumption (Fig. 7) are summarized in Table III.

Although the difference in the order parameter σ^2 can be determined from the slopes of the lines of Fig. 12, we encounter the same problem as discussed above; i.e., for some of the model compounds the k dependence of $|f(k, \pi)|$ and λ will affect the slope. Making the same simplifying assumption as before, we calculated $\sigma^2(2Q) - \sigma^2(X)$ from Eq. 7 (see Table III). The EXAFS spectra of the model compounds were taken at 300°K, whereas those of 2Q were taken at 130°K. Consequently, a thermal disorder component has to be added to σ^2 of the model compounds. Its value was determined for compound No. 5 from the slopes derived from spectra taken at 300°K and 130°K.

$$\sigma^2(300°K) - \sigma^2(130°K) = 0.0027 \pm 0.0003 \text{ Å}^2.$$

If one assumes that all the model compounds have approximately the same thermal component, 0.003 $Å^2$ must be added to the last column of Table III. The most striking feature of these results is that all values of $\sigma^2(2Q) - \sigma^2(X)$ are positive, which indicates that the Fe^{2+} site of RC is more disordered (i.e., has a larger spread in ligand distances) than that of any of the model compounds. It is also interesting that compound No. 8 of the N_2O_4 series exhibits the largest slope in Fig. 12, i.e., it is the most ordered one. This is consistent with its simple structure (see Table II), which suggests a larger number of equivalent ligands than those of compounds Nos. 7 and 9. Similarly, acetylacetonate (No. 10), which has a small spread in ligand distances (Table IV), exhibits the largest slope (line No. 8, Table III).

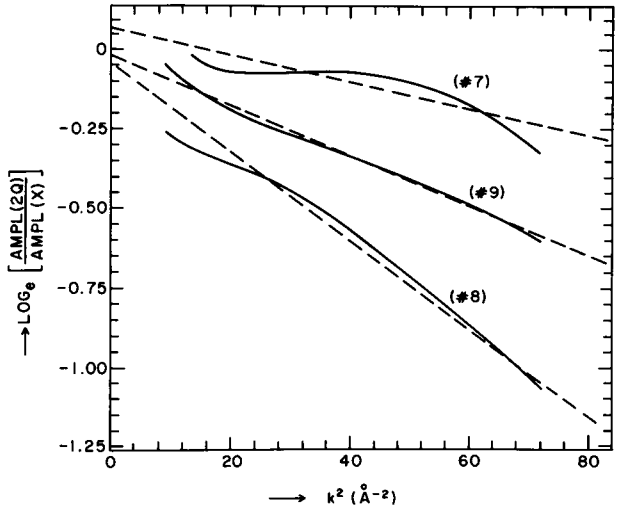

FIGURE 12 The ln of the ratio of the amplitude functions of an RC sample (2Q) to that of different model compounds versus k^2 (solid line). From the intercepts at $k = 0$, the ratio of the coordination numbers was determined (see Table III). All three model compounds have N_2O_4 ligands; they are identified by numbers in parentheses (Table II).

Control Experiments

PVA vs. Aqueous Solution. To test whether the EXAFS results depend on the matrix in which the RC

were embedded, a frozen aqueous RC sample (No. 11 in Table I) was compared with one in which the RC were embedded in PVA (No. 1 in Table I). We found that $\overline{R}$ (± 0.01 Å) as well as the amplitudes ($\Delta A/A \pm 5\%$) were the same.

Background Counts from PVA, Sucrose, and Dewar. As mentioned above in Techniques and Materials, we originally encountered a large Fe background that was traced to the blue styrofoam used in the Dewar construction. This was eliminated by replacing it with white styrofoam. The residual background counts from the Dewar were ~2% of the EXAFS signal. The background from the sucrose that was used to dilute the model compounds was found to be <2% of the signal. The background from a blank PVA sample was determined to be ~4% of the EXAFS signal. It presumably is due to an iron impurity in PVA.

Radiation Damage. Two methods were used to test the possible effects of radiation damage on the RC sample. In one, the first set of scans (~6) was averaged and compared with the last set of scans taken on the same sample. No differences were found in any of the runs. However, the conclusions arrived at from this procedure would be invalid if the radiation damage (e.g., the reduction of the quinones by photoelectrons) had occurred during the first scan. To test this possibility, optical and EPR spectra of the irradiated samples were investigated. Special samples with low optical absorbances (see Materials), were irradiated at 130°K in the EXAFS beam for different lengths of time and transferred at low temperatures (to avoid annealing of possible damage) to an optical and EPR spectrometer. The optical spectrum of an RC sample after 60 min irradiation (corresponding to ~6 scans) is shown in Fig. 13. It is indistinguishable from low temperature spectra obtained from unirradiated samples (see, for example, Fig. 1 *A* of McElroy et al., 1974). The bleaching of the far infrared peak (dashed line of Fig. 13) with strong illumination is characteristic of functional RC. The kinetics of recovery of bleaching was measured at 80°K by monitoring the light-induced EPR signal at $g = 2.0026$. The recombination time $\tau_d(1/e)$ was found to be 25 ± 3 ms, in agreement with the value found in unirradiated samples (McElroy et al., 1974). Similarly, the line shapes and positions of both the narrow $g = 2.0026$ and broad $g = 1.82$ light-induced EPR signals were found to be the same as observed in unirradiated reaction centers (Okamura et al., 1975). In addition to the light-induced signal, a second asymmetric EPR signal having a g-value of 2.0040 ± 0.0002 and linewidth of 15 gauss (peak-to-peak derivative) was observed. The same signal was observed in irradiated blank PVA samples and was, therefore, assigned to a radiation-induced damage center in PVA. From the above results, we conclude that a negligible amount of radiation damage was produced in the RC samples. These results are in agreement with those obtained by Chance et al. (1980), who showed that no significant radiation damage was produced when their EXAFS experiments were performed at low temperatures.

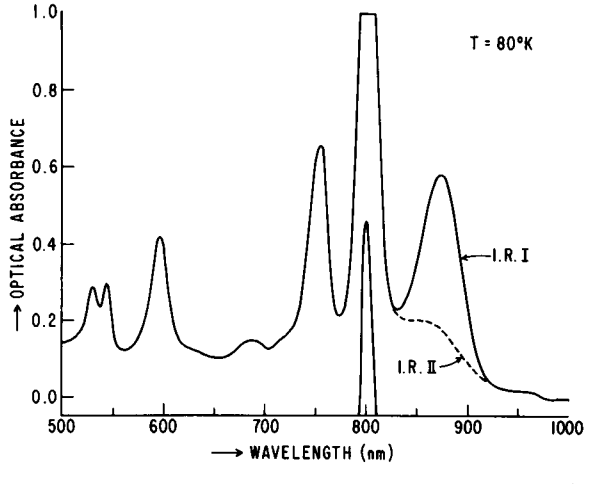

FIGURE 13 Optical spectrum at 80°K of RC sample embedded in PVA (equivalent to 1Q of Table I) after 60 min irradiation in EXAFS beam II-3. Solid line taken with weak illumination (CARY 14R, I.R.I mode), dashed line taken with strong illumination (CARY 14R, I.R.II mode). The 800-nm peak is folded over and corresponds to an absorbance of 1.47. The spectrum is indistinguishable from the one obtained from unirradiated reaction centers.

DISCUSSION AND CONCLUSIONS

The goal of this work has been to elucidate the structure of the Fe^{2+} site in photosynthetic reaction centers. The specific problems we wished to solve were the determination of (*a*) the identity of the ligands, (*b*) the number of ligands, (*c*) the average bond lengths of the ligands and the spread in their values, (*d*) the spatial relation of the quinones to the Fe^{2+} (i.e., whether or not they were ligands of Fe^{2+}), and (*e*) the possible bonding of *o*-phenanthroline to Fe^{2+}. Although we have made progress towards solving these problems, further studies will be required to obtain unequivocal answers to some of these questions.

The success of EXAFS depends to a large extent on the choice of a well characterized model compound that closely approximates the structure of the unknown sample. This becomes a difficult task when, as in the present case, one deals with a center whose structure is completely unknown. In Table III we present a comparison of some EXAFS parameters of RC with model compounds having different ligands. The problem is to decide which of them best approximates the structure of the RC. The shift of E_0 (Table III) required to fit the phase difference (see Fig. 11 and Eq. 6) depends on the electronic potential, as well as on the chemical nature of the ligands. Taking the value of $E_0(2Q) - E_0(X)$ as a rough guide, we see that the compounds with ligands N_2O_4 (Nos. 7, 8, and 9, Table III) and N_3O_3 (No. 3) require the smallest shifts. Another

rough guide is the closeness of the ratio $N(2Q)/N(X)$ to one (Table III) and the fit of the phase difference to a straight line (see the letters S and C in the fifth column of Table III). An inspection of Table III for these criteria suggests that Fe^{2+} is six coordinated with nitrogens and oxygens as ligands. It should be noted, however, from a comparison of the RC data with cyt *c* (Nos. 2 and 3, Table III) that one sulfur ligand cannot be entirely ruled out. The number of ligands (six) is in agreement with an octahedral environment that had been postulated previously from susceptibility (Butler et al., 1980) and Mössbauer (Boso et al., 1981) measurements. The lack of a significant absorption peak in the pre-edge absorption region also favors an octahedral assignment (Shulman et al., 1976). The pre-edge absorption measurements warrant a reinvestigation with higher resolution than was possible with the beam line II-3 used in these experiments.

The most striking feature of the Fe^{2+} site in RC is the large disorder parameter σ^2, which we believe to arise from large differences in bond lengths of the six Fe^{2+} ligands. The differences between the σ^2 of the RC and the model compounds are all positive (Table III), which signifies that all model compounds have fewer variations in bond lengths. The situation is even more striking when we add a thermal disorder component of 0.003 Å^2 (measured on compound No. 5) to compensate for the fact that the model compounds were run at a higher temperature (300°K) than the RC (130°K). The σ^2 of Fe^{2+} acetylacetonate (No. 11) comes closest to that of RC. This is not surprising, since Fe^{2+} acetylacetonate is known to form a complicated polymeric structure (Buckingham et al., 1967). Its crystal structure has not been determined, but that of Co II acetylacetonate is known (Cotton and Elder, 1965). The root mean square spread in ligand distances in that compound was found to be ±0.10 Å, i.e., $\sigma^2 = 0.01$ Å^2. This suggests that the static disorder parameter in RC, $\sigma^2(2Q)$, is ≥ 0.01 Å^2. An alternate estimate of $\sigma^2(2Q)$ can be made from the values of $\sigma^2(2Q) - \sigma^2(X)$ (Table III). In calculating these values, we neglected the possible contributions of $|f(k, \pi)|$ and λ. Since these can either add or subtract to the numbers in column No. 8 (Table III), we make the plausible assumption that their average contribution should cancel. Averaging all values of $\sigma^2(2Q) - \sigma^2(X)$ and adding the thermal component 0.003 Å^2 we obtain $[\sigma^2(2Q) - \sigma^2(X)]_{AVE} = 0.009$ Å^2. Since the model compounds themselves have some static disorder, we arrive at the same conclusion as before, i.e., that $\sigma^2(2Q)$ is ≥ 0.01 Å^2.

The average ligand distance $R(2Q)$ was obtained from the phase differences by a procedure outlined in the text. The results are shown in Table IV for five different model compounds. Averaging the values in Table IV we obtain

$$R(2Q) = 2.10 \pm 0.02 \text{ Å}.$$

Since the spread in distances was found to be $\geq \pm 0.1$ Å, some bond lengths will be 2.20 Å. Such long bonds are characteristic of high-spin Fe^{2+}. The average Fe^{2+}-N bond lengths of several high-spin compounds were recently determined to be: 2.161 Å (Anderson et al., 1980), 2.172 Å (Oliver et al., 1980) and 2.200 Å (Katz and Strouse, 1980). The shorter average distance found in RC is believed to be due to the presence of oxygen ligands.

The stability of the Fe^{2+} state in RC is unusual and must be connected with its environment (e.g., ligands). In most inorganic and biological molecules Fe^{2+} readily oxidizes to Fe^{3+}. The lack of negatively charged ligands (e.g., COO^-, S^-) and the presence of neutral π-acceptor ligands such as histidine nitrogens and methionine sulfurs would help stabilize the Fe^{2+} state. It seems, therefore, likely that the nitrogen ligands of Fe^{2+} in RC come from histidine rings. A more detailed analysis of this hypothesis has been performed by Bunker et al. (1981).

We turn now to the question whether the quinones are directly bound to Fe^{2+}. The first shell $k^2\chi(k)$ spectra of RC with two and one quinone were found to have the same average distance $\overline{R}$ and coordination number (Fig. 3 *a*). The simplest explanation is that the secondary quinone did not bind to Fe^{2+}, and hence its removal did not affect the spectrum. However, an alternate explanation that the quinone was bound to Fe^{2+}, and, upon removal, was replaced by another ligand (oxygen or nitrogen), cannot be excluded. Since the error in the average distance determination was ±0.01 Å, the replacing ligand can have a bond length ~0.06 Å different from the average R without significantly affecting the spectrum. This, incidentally, points to the limitation of EXAFS as a tool in trying to identify one ligand (out of six) when one is dealing with neighboring low Z ligands (i.e., C, N, O). Crystalline field parameters and quadrupole splittings are, in principle, more sensitive indicators of the local environment than the average ligand distance. These have been measured in RC by magnetic susceptibility (Butler et al., 1980) and Mössbauer spectroscopy (Boso et al., 1981). No large differences were found between RC having two and one quinones. But even in these experiments one can argue that a nearly identical ligand replaced the quinone.

Different results were observed when the primary quinone was removed. The amplitude of the 0Q sample was reduced by ~12% (see Figs. 3 *b* and 10 *b*), which is consistent with the loss of one ligand. Whether this ligand belonged to the quinone or the relatively harsh treatment (required to remove the primary quinone) broke a weak ligand cannot be determined from the EXAFS spectra. Susceptibility also showed a change in the values of the crystalline field parameters. However, the explanation that was favored involved a conformational change of the protein when the primary quinone was removed (Butler et al., 1980). This interpretation was based on EPR results that showed that the interaction of Fe^{2+} with the primary quinone was approximately the same as with the secondary quinone (Wraight, 1978; Okamura et al., 1978). A

consequence of this result is that either both or neither of the quinones ligand to Fe^{2+}. The lack of a change in the susceptibility when the secondary quinone was removed was taken as an indication that it did not ligand to Fe^{2+}. As discussed earlier, however, it is possible that an equivalent ligand replaced the quinone ligand on the Fe^{2+}. If this is indeed the case, the susceptibility and the EXAFS data are consistent with both quinones forming iron ligands. On the other hand, recent Mössbauer data (Boso et al., 1981) showed very little difference in the quadrupole splittings and isomer shifts between RC samples having one and no quinones. This result argues against the loss of a ligand. Thus, at this point no firm conclusion can be reached concerning the 0Q sample.

When the electron transfer inhibitor *o*-phenanthroline was added to RC with two and one quinones, no changes in the first shell $k^2\chi(k)$ spectra were observed (Fig. 8 *a*, *b*). However, when *o*-phenanthroline was added to 0Q*, the amplitude of the EXAFS spectrum increased to the value observed in the 2Q* and 1Q* samples (Fig. 8 *c*). This result suggests that a ligand was lost in the 0Q* sample and was now replaced by *o*-phenanthroline. However, a conformational change due to loss of the primary quinone may also be reversed by *o*-phenanthroline if this inhibitor binds at or near the quinone binding site. In trying to interpret the lack of change observed when *o*-phenanthroline was added to 2Q* and 1Q*, we encounter the same problem as discussed earlier. It is difficult to distinguish whether *o*-phenanthroline does not bind to Fe^{2+} or whether it replaces another ligand without appreciably changing $\bar{R}$. It would be instructive to explore the structure of the edge absorption region with high resolution and to compare the results obtained with 0Q, 1Q, and 2Q with those from an *o*-phenanthroline model compound.

No differences were found between the $k^2\chi(k)$ spectra of reduced (Q^-) and unreduced 1Q samples. It might also be instructive to explore the differences in the edge absorption region and to investigate carefully the shift in E_0 obtained from the phase analysis (see Table III). Both of these are affected by a change in the electronic cloud and may, therefore, shed some light on the vicinity (i.e., ligation) of the quinones to the Fe^{2+}.

In addition to the main peak in the Fourier transform (Fig. 6), a pronounced second peak was observed. Its distance was determined to be 4.14 ± 0.05 Å. This distance is too large for the second coordination shell; it must, therefore, belong to the third or higher shell. The peak corresponding to the second coordination shell may be either hidden under the side lobes of the main peak or for a variety of reasons may have too small an amplitude to be observed.

In summary, we have shown that the Fe^{2+} site in RC is structurally highly disordered. The most likely number of ligands is six made up of a mixture of oxygens and nitrogens. The average first shell ligand distance is 2.10 ± 0.02 Å, with a more distant shell at 4.14 ± 0.05 Å. The results are consistent with the Fe^{2+} being in an octahedral environment that, in view of the large spread in distances, must be highly distorted. The EXAFS results on 2Q and 1Q indicate either that the secondary quinone and *o*-phenanthroline do not bind to Fe^{2+} or that they replace an equivalent ligand. The EXAFS results on 0Q can be explained by either a loss of one ligand or a severe conformational change when the primary quinone was removed.

We thank E. Abresch for the preparation of the reaction centers, R. Isaacson for taking the EPR spectra, J. C. Smith and L. Powers for their assistance in taking some of the spectra, and K. O. Hodgson for making his laboratory available during an emergency. Special thanks are due to A. W. Addison, who synthetized many of the model compounds used in this work. We profited from several discussions and exchange of information with the University of Washington group: G. Bunker, E. A. Stern, R. E. Blankenship, and W. W. Parson.

The work of Dr. Okamura and Dr. Feher was supported by National Science Foundation grants DMR77-14659 and PCM78-13699 and National Institutes of Health grant GM 13191. The EXAFS facilities at the Stanford Synchrotron Radiation Laboratory were supported by National Science Foundation grant DMR77-27489 in cooperation with the Stanford linear accelerator and the U.S. Department of Energy.

Received for publication 28 April 1981 and in revised form 16 September 1981.

REFERENCES

Anderson, O. P., A. B. Kopelove, and D. K. Lavallee. 1980. Structure and properties of *N*-methyltetraphenylporphyrin complexes. Crystal and molecular structure and cyclic volammetry of an air-stable iron II porphyrin: chloro(*N*-methyl-5,10,15,20-tetraphenylporphinato) iron II. *Inorg. Chem.* 19:2101–2107.

Beni, G., and P. M. Platzman. 1976. Temperature and polarization dependence of extended x-ray absorption fine-structure spectra. *Phys. Rev. B.* 14:1514–1518.

Blankenship, R. E., and W. W. Parson. 1979. The involvement of iron and ubiquinone in electron transfer reactions mediated by reaction centers from photosynthetic bacteria. *Biochim. Biophys. Acta.* 545:424–444.

Boso, B., P. G. Debrunner, M. Y. Okamura, and G. Feher. 1981. Mössbauer studies of reaction centers from *R. spheroides*. *Biophys. J. (Abstr.).* 33:263*a*.

Boso, B., P. G. Debrunner, M. Y. Okamura, and G. Feher. 1981. Mössbauer spectroscopy studies of photosynthetic reaction centers from *Rhodopseudomonus sphaeroides* R-26. *Biochim. Biophys. Acta.* 638:173–177.

Buckingham, D. A., R. C. Gorges, and J. T. Henry. 1967. The polymeric nature of bis(acetylacetonato), bis(trifluoroacetylacetonato), bis(hexafluoroacetylacetonato), and bis(2,2,6,6-tetramethylheptane-3.5-dionato)-iron II. *Aust. J. Chem.* 20:281–296.

Bunker, G., E. A. Stern, R. E. Blankenship, and W. W. Parson. 1982. An x-ray absorption study of the iron site in bacterial photosynthetic reaction centers. *Biophys. J.* 37:539–551.

Butler, W. F., D. C. Johnston, H. B. Shore, D. R. Fredkin, M. Y. Okamura, and G. Feher. 1980. The Electronic structure of Fe^{2+} in reaction centers from *Rhodopseudomonas sphaeroides*. I. Static magnetization measurements. *Biophys. J.* 32:967–992.

Chan, S. I., and R. C. Gamble. 1978. X-ray absorption spectroscopy of metalloproteins. *Methods in Enzymol.* 54(part E):323–345.

Chance, B., P. Angiolillo, E. K. Yang, and L. Powers. 1980. Identification and assay of synchrotron radiation-induced alterations on metal-

loenzymes and proteins. *FEBS (Fed. Eur. Biochem. Soc.) Lett.* 112:178–182.

Citrin, P. H., P. Eisenberger, and B. M. Kincaid. 1976. Transferability of phase shifts in extended x-ray absorption fine structure. *Phys. Rev. Lett.* 36:1346–1349.

Collins, D. M., R. Countryman, and J. L. Hoard. 1972. Stereochemistry of low-spin iron porphyrins. I. Bis(imidazole)-$\alpha, \beta, \gamma, \delta$-tetraphenylporphinatoiron III chloride. *J. Am. Chem. Soc.* 94:2066–2072.

Cotton, F. A., and R. C. Elder. 1965. Crystal structure of tetrameric cobalt II acetylacetonate. *Inorg. Chem.* 4:1145–1151.

de Boor, C. 1968. On uniform approximation by splines. *Journal of Approximation Theory.* 1:219–235.

Debrunner, P. G., C. E. Schulz, G. Feher, and M. Y. Okamura. 1975. Mössbauer study of reaction centers from *R. spheroides. Biophys. J. (Abstr.)* 15:226*a*.

Debus, R. J., M. Y. Okamura, and G. Feher. 1981. Dissociation and reconstitution of the H subunit from RCs of *R. spheroides* R-26. *Biophys. J. (Abstr.)* 33:19*a*.

Doniach, S., P. Eisenberger, and K. O. Hodgson. 1980. *In* Synchrotron Radiation Research. H. Winick and S. Doniach, editors. Plenum Publishing Corp., New York. 425–458.

Eisenberger, P., and B. M. Kincaid. 1978. EXAFS: New horizons in structure determinations. *Science (Wash. D.C.).* 200:1441–1447.

Eisenberger, P., and B. Lengeler. 1980. Extended x-ray absorption fine-structure determination of coordination numbers: Limitations. *Phys. Rev. B.* 22:3551–3562.

Eisenberger, P. M., M. Y. Okamura, and G. Feher. 1980. Investigation of the ferroquinone complex in reaction centers of *R. sphaeroides* R-26 by EXAFS. *Fed. Proc. (Abstr.)* 39:1802.

Feher, G., and M. Y. Okamura. 1978. Chemical composition and properties of reaction centers. *In* The Photosynthetic Bacteria. R. K. Clayton and W. R. Sistrom, editors. Plenum Publishing Corp., New York. 349–386.

Figgis, B. N., M. Gerloch, and R. Mason. 1969. The crystallography and paramagnetic anisotropy of potassium ferricyanide. *Proc. R. Soc. A Math. Phys. Sci.* 309:91–118.

Fox, P. A., A. D. Hall, and N. L. Schryer. 1976. The PORT Library Mathematical Subroutine Library. Bell Laboratories Computing Science Technical Report No. 47.

Hastings, J. B., P. Eisenberger, B. Lengeler, and M. L. Perlman. 1979. Local-structure determination at high dilution: internal oxidation of 75-ppm Fe in Cu. *Phys. Rev. Lett.* 43:1807–1810.

Hayes, T. M., P. N. Sen, and S. H. Hunter. 1976. Structure determination using EXAFS in real space: Ge. *Proc. Phys. Soc. Lond. (Solid State Phys.).* 9:4357–4364.

Iball, J., and C. H. Morgan. 1967. A refinement of the crystal structure of ferric acetylacetonate. *Acta Crystallogr. Sect. B Struct. Crystallogr. Cryst. Chem.* 23:239–244.

Jaklevic, J., J. A. Kirby, M. P. Klein, A. S. Robertson, G. S. Brown, and P. Eisenberger. 1977. Fluorescence detection of EXAFS: sensitivity enhancement for dilute species and thin films. *Solid State Commun.* 23:679–682.

Katz, B. A., and C. E. Strouse. 1980. Spin-state isomerism of tris(2-picolylamine) iron II. the diiodide and the hydrated dichloride. *Inorg. Chem.* 19:658–665.

Kutzler, F. W., C. R. Natoli, D. K. Misemer, S. Doniach, and K. O. Hodgson. 1980. Use of one electron theory for the interpretation of near edge structure in K-shell x-ray absorption spectra of transition metal complexes. *J. Chem. Phys.* 73:3274–3288.

Lee, P. A., P. H. Citrin, P. Eisenberger, and B. M. Kincaid. 1981. Extended x-ray absorption fine structure: its strength and limitations as a structural tool. *Rev. Mod. Phys.* In press.

Lee, P. A., and G. Beni. 1977. New method for the calculation of atomic phase shifts: application to EXAFS in molecules and crystals. *Phys. Rev.* B15:2862–2883.

McElroy, J. D., D. C. Mauzerall, and G. Feher. 1974. Characterization of primary reactants in bacterial photosynthesis. II. Kinetic studies of the light-induced EPR signal ($g = 2.0026$) and the optical absorbance changes at cryogenic temperatures. *Biochim. Biophys. Acta.* 333:261–278.

Montgomery, H., R. V. Chastain, J. J. Natt, A. M. Witkowska, and E. C. Lingafelter. 1967. The crystal structure of Tutton's salts. VI. Vanadium (II), Iron (II) and Cobalt (II) ammonium sulfate hexahydrates. *Acta Crystallogr. Sect. B Struct. Crystallogr. Cryst. Chem.* 22:775–780.

Okamura, M. Y., R. A. Isaacson, and G. Feher. 1975. Primary acceptor in bacterial photosynthesis: obligatory role of ubiquinone in photoactive reaction centers of *Rhodopseudomonas sphaeroides. Proc. Natl. Acad. Sci. U. S. A.* 72:3491–3495.

Okamura, M. Y., R. A. Isaacson, and G. Feher. 1978. EPR signals from the primary and secondary quinone in reaction centers of *R. sphaeroides* R-26. *Biophys. J. (Abstr.)* 21:8*a*.

Oliver, J. D., D. F. Mullica, B. B. Hutchinson, and W. O. Milligan. 1980. Iron-nitrogen bond lengths in low-spin and high spin iron II complexes with poly(pyrazolyl) borate ligands. *Inorg. Chem.* 19:165–169.

Reed, J., P. Eisenberger, B. K. Teo, and B. M. Kincaid. 1977. Structure of the catalytic site of polymer bound Wilkinson's catalyst by X-ray absorption studies. *J. Am. Chem. Soc.* 99:5217–5218.

Rosen, D., M. Y. Okamura, and G. Feher. 1980. Interaction of cytochrome *c* with reaction centers of *Rhodopseudomonas sphaeroides* R-26: determination of number of binding sites and dissociation constants by equilibrium dialysis. *Biochemistry.* 19:5687–5692.

Shulman, R. G., P. Eisenberger, and B. M. Kincaid. 1978*a*. X-ray absorption spectroscopy of biological molecules. *Annu. Rev. Biophys. Bioeng.* 7:559–578.

Shulman, R. G., P. Eisenberger, B. K. Teo, and B. M. Kincaid. 1978*b*. Fluorescence X-ray absorption studies of rubredoxin and its model compounds. *J. Mol. Biol.* 124:305–321.

Shulman, R. G., Y. Yafet, P. Eisenberger, and W. E. Blumberg. 1976. Observation and interpretation of X-ray absorption edges in iron compounds and proteins. *Proc. Natl. Acad. Sci. U. S. A.* 73:1384–1388.

Stern, E. A., F. W. Lytle, and D. E. Sayers, 1975. Extended x-ray absorption fire structure. III. Determination of physical parameters. *Phys. Rev. B.* 11:4836–4846.

Stern, E. A. 1978. Structure determination by X-ray absorption. *Contemp. Phys.* 19:289–310.

Stern, E. A., and S. M. Held. 1979. X-ray filter assembly for fluorescence measurements of X-ray fine structure. *Rev. Sci. Instrum.* 50:1579–1582.

Stern, E., B. A. Bunker, and S. M. Held. 1980. Many-body effects on extended X-ray absorption fine structure amplitudes. *Phys. Rev.* B12:5521–5539.

Winick, H. 1980. Synchrotron radiation sources, research facilities, and instrumentation. *In* Synchrotron Radiation Research. H. Winick and S. Doniach, editors. Plenum Publishing Corp., New York. 27–58.

Winick, H., and S. Doniach, editors. 1980. Synchrotron Radiation Research. Plenum Publishing Corp., New York.

Wraight, C. 1978. Iron-quinone interactions in the electron acceptor region of bacterial photosynthetic reaction centers. *FEBS (Fed. Eur. Biochem. Soc.) Lett.* 93:283–288.

Wyckoff, R. W. G. 1963. Crystal Structures. John Wiley & Sons, New York. Vol. 5.